ARTICLE IN PRESS

Journal of the European Ceramic Society xxx (xxxx) xxx



Contents lists available at ScienceDirect

Journal of the European Ceramic Society

journal homepage: www.elsevier.com/locate/jeurceramsoc



Short communication

High-temperature oxidation and nitridation of substoichiometric zirconium carbide in isothermal air

Matthew T. Konnik ^{a,b,*}, Trey Oldham ^{a,c}, Allison Rzepka ^{a,b}, Vincent Le Maout ^{a,b}, Kelly A. Stephani ^{a,b}, Francesco Panerai ^{a,c}

- a Center for Hypersonics and Entry Systems Studies, University of Illinois at Urbana-Champaign, Urbana, IL, 61801, USA
- b Department of Mechanical Science and Engineering, University of Illinois at Urbana-Champaign, Urbana, IL, 61801, USA
- ^c Department of Aerospace Engineering, University of Illinois at Urbana-Champaign, Urbana, IL, 61801, USA

ARTICLE INFO

Keywords: UHTC Oxidation Nitridation Zirconia High-temperature

ABSTRACT

The influence of nitrogen on the oxidation behavior of hot-pressed zirconium carbide was investigated using a flow-tube furnace at temperatures ranging from 1000 to 1600 °C. Mass gain, oxide formation characteristics, and oxide transitions were evaluated at various experimental conditions. Differences in oxidation behavior across the range of temperatures investigated show both kinetic and microstructural dependence with implications pointing to this materials efficacy in ultra-high temperature applications. Results suggest that at temperatures above 1400 °C, although oxidation mechanisms remain dominant, nitridation and reduction mechanisms may be appreciable enough to require consideration. Supporting discussions regarding polymorphism and microstructural influences are outlined.

Ultra-high temperature (UHT) materials have garnered research interest in applications spanning hypersonics, nuclear engineering, and manufacturing due to their unique ability to withstand harsh environments. Zirconium carbide (ZrC_x), a transition metal carbide, is a promising UHT material owing to the excellent thermal, mechanical, and chemical properties it possess [1–5]. Despite these advantages, reports on the material response of ZrC_x at higher temperatures are limited, often resulting in the usage of better understood transition metal carbides and borides [6]. In particular, the thermochemical response of UHT materials in nitrogen and oxygen, being the main constituents of air, are some of the most important behavioral characteristics to understand. Yet, this has not been thoroughly characterized for ZrC_x at high temperatures.

Numerous breakthrough studies on the response of ZrC_x to oxygen have been performed in the last century and have chronologically investigated higher temperatures. Kuriakose et al. investigated the kinetics of ZrC_x oxidation in a heated flow chamber, but were limited to the range of 554–652 °C due to the mechanical stability of the oxide layer formed [7]. Shimada et al. investigated both isothermal and non-isothermal furnace oxidation of ZrC_x powders from 380 to 550 °C with oxygen partial pressures ranging from 1.3 to 7.9 kPa under 39.5 kPa total static pressure [8]. Rama Rao et al. explored ZrC_x oxidation at temperatures of up to 800 °C [9] and more recently, Gasparrini et al. studied oxidation kinetics in a laboratory furnace at temperatures of up to 1100 °C [10]. Few studies have been performed

at elevated temperatures (up to 1800 °C), yet these were performed in an O_2 environment at very low pressures [11]. Wuchina and Opeka have also reviewed the oxidation properties of ZrC_x [12]. Each study has observed some aspect of a two-phase oxidation mechanism through oxycarbide formation and carbon precipitation subsequently leading to ZrO_2 formation. Though, numerous differences exist regarding reported kinetics, as well as resulting microstructure and morphologies of the scale, likely due to differences in substrate stoichiometry, impurity concentration and test environment.

Nitridation of ZrC_x is much less studied, yet the effects can be drastic. Kieffer et al. investigated the nitridation behavior of transition metal carbides in an autoclave furnace from 1400 to 1800 °C at 1 to 300 atm, reporting carbide to nitride conversions of up to 80 mol% [13]. A few other studies have also been performed in nitrogen atmospheres up to 2500 °C, all with similar findings regarding the transition of carbide to carbonitride and nitride phases [14–17].

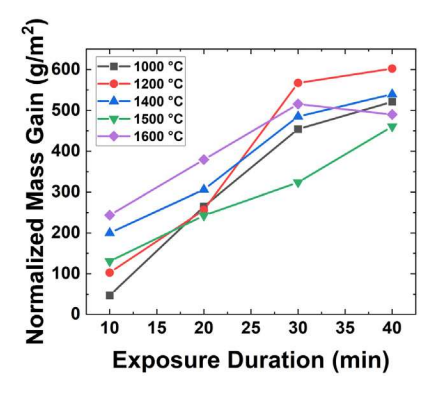
While there has been work on both the oxidation and nitridation of ${\rm ZrC}_x$, there is little to no discussion on how one can influence another. In order to understand the role nitrogen exposure can have on the oxidation of ${\rm ZrC}_x$, as well as provide some of the first oxidation data available beyond 1100 °C at atmospheric pressure, this work focuses on furnace experiments in which a ${\rm ZrC}_x$ substrate is pre-treated in nitrogen before air oxidation.

https://doi.org/10.1016/j.jeurceramsoc.2024.04.006

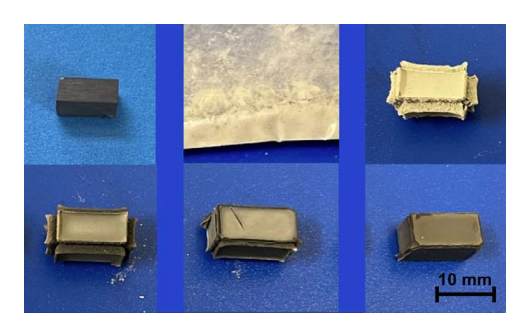
Received 5 January 2024; Received in revised form 29 March 2024; Accepted 3 April 2024 Available online 4 April 2024

0955-2219/© 2024 The Author(s). Published by Elsevier Ltd. This is an open access article under the CC BY-NC-ND license (http://creativecommons.org/licenses/by-nc-nd/4.0/).

^{*} Corresponding author at: Department of Mechanical Science and Engineering, University of Illinois at Urbana-Champaign, Urbana, IL, 61801, USA. E-mail address: mkonnik2@illinois.edu (M.T. Konnik).



(a) Normalized mass gain plotted versus exposure duration for specified oxidation temperatures.



(b) Top row, left to right: unoxidized specimen, 1000 $^{\circ}$ C, 1200 $^{\circ}$ C. Bottom row, left to right: 1400 $^{\circ}$ C, 1500 $^{\circ}$ C. All oxidized specimens exposed for 40 minutes.

Fig. 1. Mass gain versus time profile and examples of test specimens.

Table 1As-recieved ZrC, parameters.

C:Zr ratio	Purity	Porosity
0.63	99.9%	12%

 $\rm ZrC_x$ sputtering targets (99.9%, MSE Supplies) were used as received to create test specimens sized 12.5 × 6 × 6 mm. Note the target was fabricated using hot isostatic pressing at 2273 K. Specimens were sectioned from the bulk material using a low speed precision cutter (IsoMet) attached with a diamond sectioning blade (IsoMet 20 LC, Buehler). Verification of the $\rm ZrC_x$ system, described in Table 1, was confirmed as explained in Supplementary Note I of the supplementary information (SI).

Oxidation experiments were performed in a horizontal tube furnace (CM 1730, CM Furnaces Inc.). Test specimens were then placed in a high-purity alumina crucible and inserted into the furnace. The furnace was then ramped to temperature (at a rate of 200 °C/h up to 800 °C and 100 °C/h thereafter) while flowing 2 lpm of nitrogen (measured using a variable area flow meter). Upon reaching the desired temperature (1000 to 1600 °C), gas composition was changed to a mixture of 20% oxygen and 80% nitrogen (0.4 lpm $\rm O_2$, 1.6 lpm $\rm N_2$) for the desired exposure duration (10 to 40 min). Upon completion of the desired oxidation exposure time, gas flow was switched back to nitrogen and the furnace was ramped down to room temperature with an identical ramp profile. Samples mass and dimensions were recorded prior to and after furnace exposure.

Samples were then analyzed using scanning electron microscopy (SEM, Quanta FEG 450 ESEM, FEI Company), x-ray photoelectron spectroscopy (XPS, Kratos Axis ULTRA, Kratos Analytical), and x-ray diffraction (Cu K- α source; D8 Advance; Bruker Corporation) according to details described in Note II of the SI.

Fig. 1(a) shows total mass gain, as a relative percentage, versus air exposure duration, a test matrix is available in Section III of the SI. The 1000 °C 10 min condition was run in triplet and the standard deviation of normalized mass gain found to be 11.64 g m $^{-2}$. Varying the exposure duration of $\rm ZrC_x$ specimens in high temperature oxidizing environments revealed cross-over in relative mass gain across the time series, suggesting a deviation from a pure Arrhenius rate form (as would be seen in pure oxygen). As exposure duration increases, the lower temperature regime begins to dominate in total mass increase, pointing to a relative slowdown in oxidation at higher temperatures. Specifically, specimens oxidized at 1200 °C overtake higher oxidation temperature mass gains for exposure durations longer than 20 min. We find that kinetic, morphological, and microstructural deviations across

temperatures are likely all major contributors to the observed mass gain behavior.

The set of competing reactions occurring during ZrC_x oxidation are given by [10]:

$$ZrC + \frac{1}{2}(1 - x)O_{2(g)} \longrightarrow ZrC_xO_{1-x} + (1 - x)C$$
 (1)

$$ZrC_xO_{1-x} + \frac{1}{2}(1+3x)O_{2(g)} \longrightarrow ZrO_2 + (x)CO_{2(g)}$$
 (2)

$$C + O_{2(g)} \longrightarrow CO_{2(g)}$$
 (3)

Reaction (1) describes the conversion at the reaction front and interfacial region, capable of producing stable zirconium oxicarbides, zirconia, and free carbon. Reaction (2) describes the production of zirconia from any oxycarbide formations, which is accompanied by carbon dioxide outgassing. Reaction (3) describes a separate mechanism for which free carbon formations present in the substrate or intermediate layer can form gaseous carbon dioxide independently of zirconia formation. The reaction in Eq. (1) describes a reaction that only produces solid state products, unlike Eqs. (2) and (3) lead to gaseous by-products while resulting in a net mass gain or mass loss, respectively. The consequence is that a small deviation in kinetic rate dependence with temperature between these three reaction mechanisms can lead to large deviations in mass gain behavior.

Any nitridation occurring prior to oxygen exposure introduces further complexity by altering the activation energy and structure associated with the aforementioned oxidation mechanisms. Preliminary furnace experiments performed under pure nitrogen provided evidence of a direct nitridation mechanism, such as that described in Eq. (4), active at the temperatures in this study. Given that furnace ramp rate is constant, each oxidation temperature explored is associated with a different nitrogen exposure duration, which combined with varying temperatures leads to dissimilar degrees of nitridation in the substrate. When considering a substoichiometric ZrC_x , increasing degrees of nitrogen incorporation into carbon vacancy cites through intermediate pathways of Eq. (4) is likely to increase the oxidation resistance of the substrate, contributing to the suppressed mass gain of higher temperatures observed in Fig. 1(a).

$$2\operatorname{ZrC} + \operatorname{N}_{2(g)} \longrightarrow 2\operatorname{ZrN} + 2\operatorname{C} \tag{4}$$

Fig. 2 shows high resolution XPS scans for each specimen treated in air for 20 min at increasing temperatures. Where applicable, the spot was focused on a cross section of the sample encompassing the reaction front and surroundings (see SI Note IV for details). Cross sections were prepared for XPS by first sectioning with an IsoMet 20 LC diamond

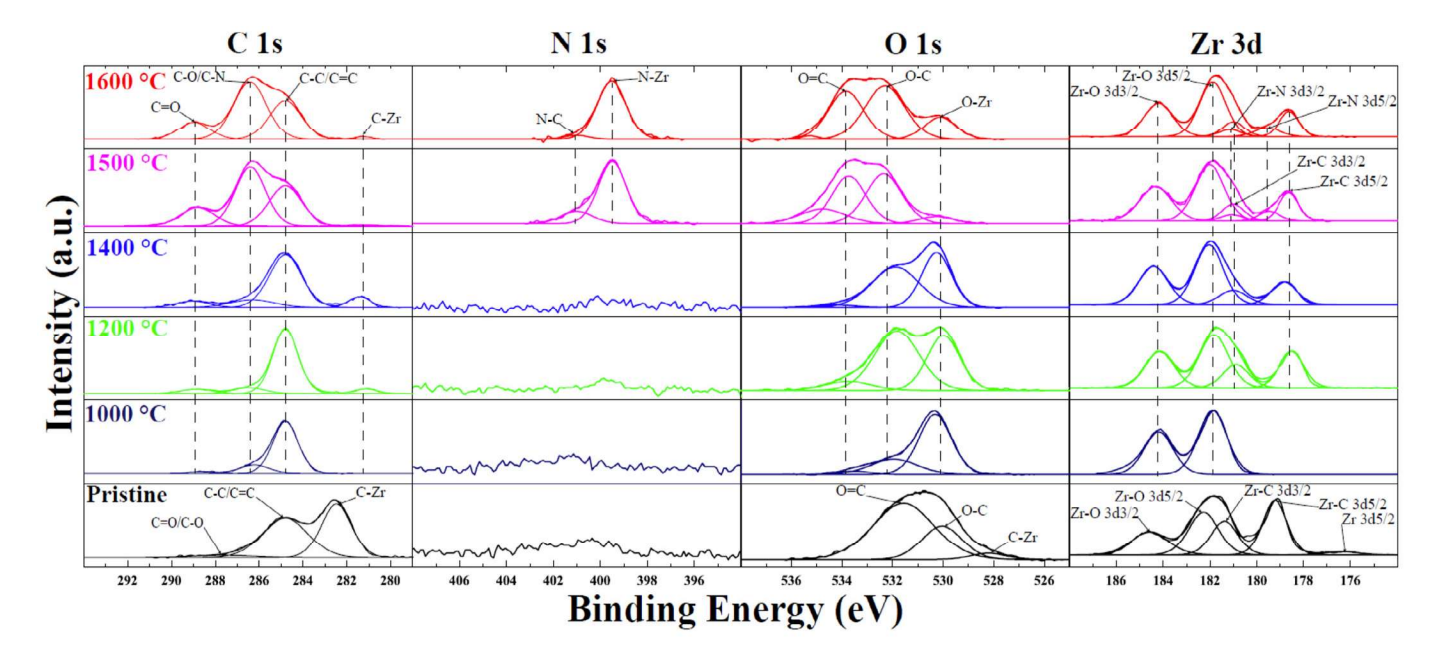


Fig. 2. X-ray photoelectron spectroscopy high resolution scans and fits of the C1s, N1s, O1s, and Zr3d orbitals. Each row is associated with a specimen treated for 20 min (if applicable) at conditions designated on the left.

blade, followed by SiC polishing to 1200 grit, and lapped with diamond films down to 3 μm . Specimens were cleaned in an ultrasonic bath of isopropanol and outgassed in between preparation steps. For the 1000 °C oxidation case, the collected powder was analyzed as the scale had no mechanical integrity. The majority of XPS signal was attributed to Zr–C, Zr–O, C–C, and typical adventitious carbon associations [18–28]. For samples exposed to higher than 1400 °C, analysis showed an uptake in N1s signal and a corresponding perturbation in the Zr3d signal around 179.5 eV, consistent with the presence of a metallic Zr–N type bonding [29–31] . Drastic increases in the carbonyl and C–O/C–N groups were also present in this temperature regime, which requires further investigation.

Observation of Zr-N type bonding above 1400 °C suggests that the ZrC_x substrate may have been sufficiently nitridated during furnace ramp up such that not all nitrogen-containing compounds were consumed during oxidation. Though, the combined carbothermic-reduction nitridation (Eq. (5)) mechanism often seen in the synthesis of ZrN using a ZrO₂ precursor [32,33] remains plausible given the production of free carbon during ZrO₂ formation (Eq. (1)) [1,8,9,34] and the dominant presence in the C1s signal in the XPS spectra shown in Fig. 2. It is crucial to note that the oxidation of ZrCx at temperatures exceeding 1400 °C approaches the minimum temperatures used in the synthesis of ZrCx and ZrN, which typically leverage a carbothermic reduction or combined reduction-nitridation mechanism of ZrO₂ [35-37]. While synthesis of these products is usually performed by homogenizing ZrO₂ and carbon graphite powders and heating in an inert environment, an oxidizing environment can produce the same conditions locally at the ZrC_x-ZrO₂ interface where solid state and gaseous carbon products are created during oxidation or direct nitridation. While the XPS results provide compelling evidence of nitridation mechanisms at these temperatures, the decrease in the overall mass gain of furnace specimens from 30 and 40 min at 1600 °C is further indication of active reduction mechanisms. As such, during air exposure of ZrCx above 1400 °C on relevant timescales, the process described in Eqs. (1)-(3), can be accompanied by nitridation and carbothermal reduction mechanisms, as presented in synthesis literature [33,38], described in Eqs. (5)–(6):

$$2\operatorname{ZrO}_2 + \operatorname{N}_{2(g)} + 4\operatorname{C} \longrightarrow 2\operatorname{ZrN} + 4\operatorname{CO}_{(g)}$$
 (5)

$$ZrO_2 + 3C \longrightarrow ZrC + 2CO_{(g)}$$
 (6)

These reaction mechanisms and their intermediate steps, compete with the oxidation processes in Eqs. (1)–(3) to describe the deviations in mass gain dominance in temperature and time observed Fig. 1(a). While slowed down by the processes described in (4)–(6), mass gain via oxidation remains predominant across the entire temperature range investigated, as clearly shown by the $\rm ZrO_2$ signal in the XPS scans, and also in the XRD measurements shown later in Fig. 3. Reduction mechanisms may manifest themselves in mass gain data as a response to long exposures where reaction front oxygen flux drops off in time due to oxide growth.

The kinetics discussed thus far are further influenced by the evolving morphology of the oxide. Zirconia equilibrium phases are well known; monoclinic zirconia (m-ZrO2) is stable at and above room temperature, and that tetragonal zirconia (t-ZrO₂) is stable at temperatures between roughly 1173 °C and 2360 °C on heating and 987 °C and 2360 °C on cooling at atmospheric pressure [39-41]. Although the temperatures for pre-existing zirconia morphologies are relatively well defined, preferential zirconia phase nucleation with temperature during ZrC_x oxidation are less understood. Fig. 1(b), shows specimen oxide formations across a range of temperatures exposed for 40 min. Drastic differences in both the appearance and mechanical integrity of the oxide layer formation exist in temperature. Both these features can be attributed to the zirconia morphology developed during oxidation, phase transition (if any) and accompanying Martensistic transformation, which introduces high mechanical integrity by way of residual stress formation in the oxide [42], on cooling. A discussion on the mechanical integrity of oxide formations is presented in Supplementary Note V of the SI.

While the temperatures explored in this study are too high for many x-ray diffractometers to observe nucleation of ZrO₂ in-situ, a footprint of the previous morphology can still be found, allowing for a more definitive metric of evaluation. Whereas the majority of the oxide formation undergoes a phase-transformation to m-ZrO₂ on cooling, some stabilized t-ZrO₂ crystallite formations which nucleated during oxidation at temperature remain after cooling. Fig. 3 shows

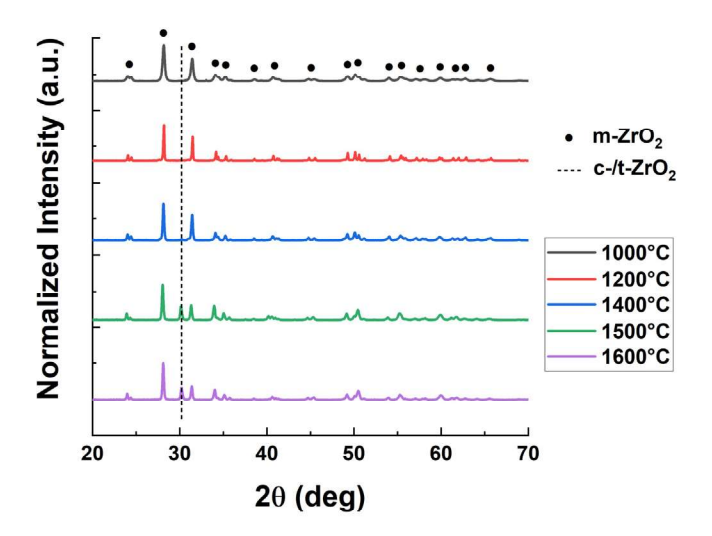


Fig. 3. X-ray diffraction profiles of the surface of oxide formations associated with each temperature investigated. Profiles shown were extracted from 30 min exposure test specimens.

this phenomenon by way of XRD analyses performed at room temperature, post-oxidation on the surface of the oxide scale. For the specimens oxidized at a sufficiently high temperature (1400–1600 °C), these tetragonal crystallites are visible at a 2θ angle of 30.26 degrees, suggesting the presence of a stabilizing agent, such as nitrogen, integrated in the t-ZrO₂ lattice [43–45]. In contrast, for specimens oxidized below the nucleation temperature required to form a sufficient quantity of t-ZrO₂ (1000 and 1200 °C), there is no signature present. These observations were found to be independent of exposure duration.

It is unknown how drastically morphological differences across temperature alter rate coefficients, but differences in formation energy and lattice configuration, transformation toughening (when oxidizing at temperatures fluctuating around phase transition temperatures), local density differences in the oxide due to variation in morphology, and increased crystallite dislocations and defects due to polymorphic zirconia formation can all play a part. While these morphological aspects can influence the effective chemical kinetics, microstructural dependencies on temperature can also be coupled to these phenomena.

Fig. 4 shows example micrographs of pore formations in oxide formations (after sectioning and polishing of sufficiently high mechanical integrity specimens) across temperatures with corresponding binary images formed from thresholding. Binary images were then used to form approximations for resulting porosity in the field of view (assuming isotropic pore formations). Resulting porosity approximations are averages over at least three 200 μ m field of view images per exposure duration, and over at least two exposure durations per temperature. Given this approach, porosities in zirconia formations created at 1200, 1400, 1500, and 1600 °C are determined to be 35%, 18%, 2.5%, and 2%, respectively.

Aside from the morphological aspects, the porosity of an oxide formation can be impacted by grain growth size at a given temperature. Grain boundary mobility is influenced by and proportional to temperature, meaning that larger crystallites will form at higher oxidation temperatures [46]. With larger grains at higher temperatures, comes a smaller total grain boundary area. Then at higher temperatures, a reactants diffusion into the material, and outflow of gaseous oxidation by-products have less opportunity to initiate pore formation. In contrast, at lower temperatures with smaller crystal formations, total grain boundary area is relatively high (by way of a larger number of formations), giving a higher probability for gaseous products to

form pores at temperature. This method of void formation in the oxide is, of course, tied to the kinetics by way of carbon outgassing rate and differential concentration of oxygen. In turn, these quantities are dependent on porosity and tortuosity of the oxide formation.

In this study, we have investigated the high temperature oxidation response of zirconium carbide specimens in the presence of a constant nitrogen flow, using a flow-tube furnace environment. Relative mass gain versus exposure duration profiles were obtained for temperatures ranging from 1000 to 1600 °C and the kinetic, morphological, and microstructural influences were discussed. Nitridation and reduction mechanisms were found to be influential in the material response, especially at sufficiently high temperatures, suppressing the expected rate of mass gain above 1200 °C. These processes take place primarily in the scale-substrate interfacial region, as suggested by the presence of a nitride phase observed in cross section analyses, but not in external scale investigations. Phase transitions and polymorphism affecting the specimens at the studied temperatures also present an influence on the quality of oxide formed, as well as potential influence on mass gain through differing formation energies and defect modes. Finally, porosity differences in oxide formations were found to be as high as 32%, with a decreasing trend in porosity with increasing temperature, creating a dense, potentially passivating oxide formation (depending on specimen geometry) at temperatures in excess of 1400 °C. Observations presented in this work act as the only current investigation regarding the influence of nitrogen on the bulk oxidation of zirconium carbide at ultra-high temperatures. This work further serves also as a basis for future investigations across the regimes which influence aggregate thermochemical response behavior of zirconium carbides and potential nitrogen treatments to alter oxidation properties and scale quality.

CRediT authorship contribution statement

Matthew T. Konnik: Conceptualization, Data curation, Formal analysis, Investigation, Methodology, Resources, Validation, Visualization, Writing – original draft, Writing – review & editing. Trey Oldham: Conceptualization, Formal analysis, Resources, Visualization, Writing – review & editing. Allison Rzepka: Conceptualization, Resources, Writing – review & editing. Vincent Le Maout: Conceptualization, Resources, Writing – review & editing. Kelly A. Stephani: Conceptualization, Funding acquisition, Methodology, Project administration, Resources, Supervision, Writing – review & editing. Francesco Panerai: Conceptualization, Funding acquisition, Methodology, Project administration, Resources, Supervision, Writing – review & editing.

Declaration of competing interest

The authors declare that they have no known competing financial interests or personal relationships that could have appeared to influence the work reported in this paper.

Acknowledgments

The work presented in this article was supported by Lockheed Martin Cooperation under grant LMC #S20-005. The authors acknowledge the use of facilities and instrumentation at the Materials Research Laboratory Central Research Facilities, University of Illinois, partially supported by NSF through the University of Illinois Materials Research Science and Engineering Center DMR-1720633. The authors would also like to thank Dan Hecht from Lockheed Martin for his guidance and many fruitful discussions.

Appendix A. Supplementary data

Supplementary material related to this article can be found online at https://doi.org/10.1016/j.jeurceramsoc.2024.04.006.

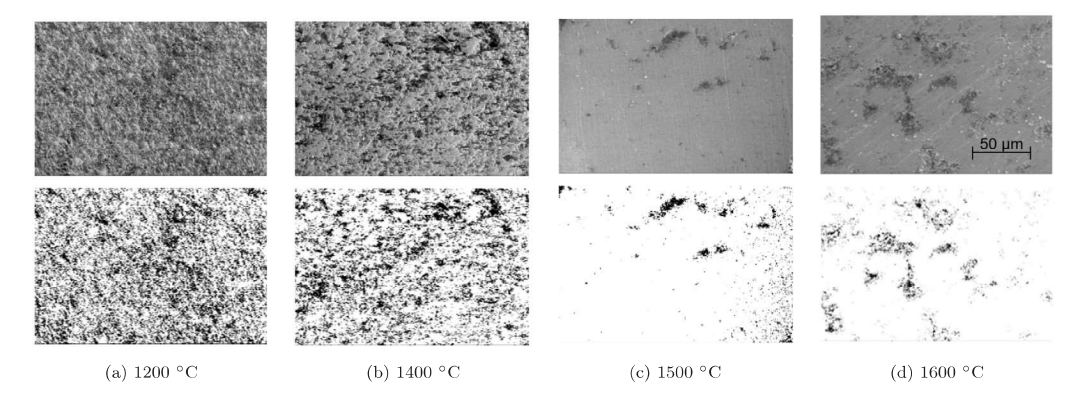


Fig. 4. Example micrographs and corresponding binary images of oxide formations from sectioned and polished specimens exposed to oxygen for 20 min at designated temperatures.

References

- Y. Katoh, G. Vasudevamurthy, T. Nozawa, L.L. Snead, Properties of zirconium carbide for nuclear fuel applications, J. Nucl. Mater. 441 (2013) 718–742, http://dx.doi.org/10.1016/j.jnucmat.2013.05.037.
- [2] Y. Wang, Q. Liu, J. Liu, L. Zhang, L. Cheng, Deposition mechanism for chemical vapor deposition of zirconium carbide coatings, J. Am. Ceram. Soc. 91 (2008) 1249–1252, http://dx.doi.org/10.1111/j.1551-2916.2007.02253.x.
- [3] W.A. Mackie, P.R. Davis, Single-crystal zirconium carbide as a high-temperature thermionic cathode material, IEEE Trans. Electron Devices 36 (1989) 220–224, http://dx.doi.org/10.1109/16.21209.
- [4] M. Caccia, M. Tabandeh-Khorshid, G. Itskos, A.R. Strayer, A.S. Caldwell, S. Pidaparti, S. Singnisai, A.D. Rohskopf, A.M. Schroeder, D. Jarrahbashi, T. Kang, S. Sahoo, N.R. Kadasala, A. Marquez-Rossy, M.H. Anderson, E. Lara-Curzio, D. Ranjan, A. Henry, K.H. Sandhage, Ceramic-metal composites for heat exchangers in concentrated solar power plants, Nature 562 (2018) 406–409, http://dx.doi.org/10.1038/s41586-018-0593-1.
- [5] M.M. Opeka, I.G. Talmy, E.J. Wuchina, J.A. Zaykoski, S.J. Causey, Mechanical, thermal, and oxidation properties of refractory hafnium and zirconium compounds, J. Eur. Ceram. Soc. 19 (13–14) (1999) 2405–2414, http://dx.doi.org/10.1016/S0955-2219(99)00129-6.
- [6] W.G. Fahrenholtz, G.E. Hilmas, Ultra-high temperature ceramics: Materials for extreme environments, Scr. Mater. 129 (2017) 94–99, http://dx.doi.org/10.1016/ j.scriptamat.2016.10.018.
- [7] A.K. Kuriakose, J.L. Margrave, The oxidation kinetics of zirconium diboride and zirconium carbide at high temperatures, J. Electrochem. Soc. 111 (1964) 827–831
- [8] S. Shimada, Oxidation kinetics of zirconium carbide at relatively low temperatures, J. Am. Ceram. Soc. 73 (1990).
- [9] G.A.R. Rao, V. Venugopal, Kinetics and mechanism of the oxidation of ZrC, J. Alloys Compd. 206 (1994) 237–242.
- [10] C. Gasparrini, R.J. Chater, D. Horlait, L. Vandeperre, W.E. Lee, Zirconium carbide oxidation: Kinetics and oxygen diffusion through the intermediate layer, J. Am. Ceram. Soc. 101 (2018) 2638–2652, http://dx.doi.org/10.1111/jace.15479.
- [11] I.L. Shabalin, Zirconium monocarbide, in: Ultra-High Temperature Materials II, Springer Nature Singapore Pte Ltd., Singapore, 2019, pp. 562–567, http://dx.doi.org/10.1007/978-94-024-1302-1.
- [12] E.J. Wuchina, M. Opeka, The group IV carbides and nitrides, in: W.G. Fahrenholtz, E.J. Wuchina, W.E. Lee, Y. Zhou (Eds.), Ultra-High Temperature Ceramics, John Wiley & Sons, Inc, Hoboken, NJ, 2014, pp. 361–390, http://dx.doi.org/10.1002/9781118700853.ch14.
- [13] R. Kieffer, H. Nowotny, P. Ettmayer, M. Fruedhofmeier, Über die beständigkeit von übergangsmetallcarbiden gegen stickstoff bis zu 300 at, Monatsh. Chem. 101 (1970) 62–82.
- [14] G. Klimashin, A. Avgustinik, G. Smirnov, Karbonitridnye i oksikarbidnye fazy titana i tsirkoniya, SSSR Neorg. Mater. 8 (5) (1972) 843–845.
- [15] Y. Vilk, I. Danisia, Y. Inekchenko, T. Ryzhkova, Variations of certain physico-chemical properties in the system zirconium carbide zirconium nitride, Russ. J. Appl. Chem. 41 (4) (1968) 873–881.
- [16] V. Neshpor, Y. Vilk, I. Danisia, Change in the electro- and thermophysical properties in pseudobinary alloys along the ray ZrC_{0.92}-ZrN_{0.85} of the zirconium-nitrogen-carbon system, Powder Metall. Met. Ceram. 6 (1) (1967) 68–71.
- [17] S. Binder, W. Lengauer, P. Ettmayer, J. Bauer, J. Debuigne, M. Bohn, Phase equilibra in the systems Ti - C - N, Zr - C - N and Hf - C - N, J. Alloys Compd. 217 (1) (1995) 128–136.
- [18] Y. Long, A. Javed, J. Chen, Z.-k. Chen, X. Xiong, Phase composition, microstructure and mechanical properties of ZrC coatings produced by chemical vapor deposition, Ceram. Int. 40 (1, Part A) (2014) 707–713, http://dx.doi.org/10.1016/j.ceramint.2013.06.059.

- [19] K.L. Håkansson, H.I.P. Johansson, L.I. Johansson, High-resolution core-level study of ZrC(100) and its reaction with oxygen, Phys. Rev. B 48 (4) (1993) 2623–2626, http://dx.doi.org/10.1103/PhysRevB.48.2623.
- [20] L. Hou, Q. Liang, F. Wang, Mechanisms that control the adsorption-desorption behavior of phosphate on magnetite nanoparticles: the role of particle size and surface chemistry characteristics, RSC Adv. 10 (4) (2020) 2378–2388, http: //dx.doi.org/10.1039/C9RA08517C.
- [21] D. Majumdar, D. Chatterjee, X-ray photoelectron spectroscopic studies on yttria, zirconia, and yttria-stabilized zirconia, J. Appl. Phys. 70 (2) (1991) 988–992, http://dx.doi.org/10.1063/1.349611.
- [22] S. Sinha, S. Badrinarayanan, A. Sinha, An XPS study of hydrogen implanted zirconium, J. Less Common Met. 134 (2) (1987) 229–236, http://dx.doi.org/10. 1016/0022-5088(87)90562-5.
- [23] L. Kumar, D. Sarma, S. Krummacher, XPS study of the room temperature surface oxidation of zirconium and its binary alloys with tin, chromium and iron, Appl. Surf. Sci. 32 (3) (1988) 309–319, http://dx.doi.org/10.1016/0169-4332(88)90016-5.
- [24] D. Sarma, C. Rao, XPES studies of oxides of second- and third-row transition metals including rare earths, J. Electron Spectrosc. Relat. Phenom. 20 (1) (1980) 25-45. http://dx.doj.org/10.1016/0368-2048(80)85003-1.
- [25] D.J. Morgan, Comments on the XPS analysis of carbon materials, C 7 (3) (2021) 51, http://dx.doi.org/10.3390/c7030051.
- [26] D. Hauser, A. Auer, J. Kunze-Liebhäuser, S. Schwarz, J. Bernardi, S. Penner, Hybrid synthesis of zirconium oxycarbide nanopowders with defined and controlled composition, RSC Adv. 9 (6) (2019) 3151–3156, http://dx.doi.org/10. 1039/C8RA09584A.
- [27] H. Gu, J. Ding, Q. Zhong, Y. Zeng, F. Song, Promotion of surface oxygen vacancies on the light olefins synthesis from catalytic CO₂ hydrogenation over FeK/ZrO₂ catalysts, Int. J. Hydrogen Energy 44 (23) (2019) 11808–11816, http://dx.doi.org/10.1016/j.ijhydene.2019.03.046.
- [28] S. Liu, X. Wu, J. Tang, P. Cui, X. Jiang, C. Chang, W. Liu, Y. Gao, M. Li, D. Weng, An exploration of soot oxidation over CeO₂-ZrO₂ nanocubes: Do more surface oxygen vacancies benefit the reaction? Catal. Today 281 (2017) 454–459, http://dx.doi.org/10.1016/j.cattod.2016.05.036.
- [29] A. Ul-Hamid, The effect of deposition conditions on the properties of Zr-carbide, Zr-nitride and Zr-carbonitride coatings – a review, Mater. Adv. 1 (5) (2020) 988–1011, http://dx.doi.org/10.1039/D0MA00232A.
- [30] S. Badrinarayanan, S. Sinha, A. Mandale, XPS studies of nitrogen ion implanted zirconium and titanium, J. Electron Spectrosc. Relat. Phenom. 49 (3) (1989) 303–309, http://dx.doi.org/10.1016/0368-2048(89)85018-2.
- [31] S. Calderon V, A. Cavaleiro, S. Carvalho, Chemical and structural characterization of ZrCNAg coatings: XPS, XRD and Raman spectroscopy, Appl. Surf. Sci. 346 (2015) 240–247, http://dx.doi.org/10.1016/j.apsusc.2015.03.161.
- [32] B. Fu, L. Gao, Synthesis of nanocrystalline zirconium nitride powders by reduction-nitridation of zirconium oxide, J. Am. Ceram. Soc. 87 (4) (2004) 696–698, http://dx.doi.org/10.1111/j.1551-2916.2004.00696.x.
- [33] S. Zhao, J. Ma, R. Xu, X. Lin, X. Cheng, S. Hao, X. Zhao, C. Deng, B. Liu, Synthesis and characterization of zirconium nitride nanopowders by internal gelation and carbothermic nitridation, Sci. Rep. 9 (1) (2019) 19199, http://dx.doi.org/10.1038/s41598-019-55450-x.
- [34] J. David, G. Trolliard, M. Gendre, A. Maître, TEM study of the reaction mechanisms involved in the carbothermal reduction of zirconia, J. Eur. Ceram. Soc. 33 (1) (2013) 165–179, http://dx.doi.org/10.1016/j.jeurceramsoc.2012.07.
- [35] X. Sun, C. Deng, J. Ma, X. Zhao, S. Hao, Z. Li, B. Liu, The study of carbothermic reduction–sintering of ZrO₂–ZrC–C composite microspheres prepared by internal gelation, J. Mater. Sci. 53 (20) (2018) 14149–14159, http://dx.doi.org/10.1007/ s10853-018-2646-0.
- [36] A. Sondhi, C. Morandi, R. Reidy, T. Scharf, Theoretical and experimental investigations on the mechanism of carbothermal reduction of zirconia, Geram. Int. 39 (4) (2013) 4489–4497, http://dx.doi.org/10.1016/j.ceramint.2012.11.043.

ARTICLE IN PRESS

M.T. Konnik et al.

Journal of the European Ceramic Society xxx (xxxx) xxx

- [37] R.W. Harrison, W.E. Lee, Processing and properties of ZrC, ZrN and ZrCN ceramics: a review, Adv. Appl. Ceram. 115 (5) (2016) 294–307, http://dx.doi.org/10.1179/1743676115Y.0000000061.
- [38] A.J. Parkison, A.T. Nelson, Deconvolution of mass gain and mass loss mechanisms during carbothermic reduction to nitridation of zirconia, J. Am. Ceram. Soc. 99 (5) (2016) 1525–1533, http://dx.doi.org/10.1111/jace.14156.
- [39] T. Götsch, W. Wallisch, M. Stöger-Pollach, B. Klötzer, S. Penner, From zirconia to yttria: Sampling the YSZ phase diagram using sputter-deposited thin films, AIP Adv. 6 (2016) http://dx.doi.org/10.1063/1.4942818.
- [40] M. Gurak, Q. Flamant, L. Laversenne, D.R. Clarke, On the Yttrium Tantalate Zirconia phase diagram, J. Eur. Ceram. Soc. 38 (2018) 3317–3324, http://dx.doi.org/10.1016/j.jeurceramsoc.2018.03.012.
- [41] S. Block, J.A.H.D. Jornada, G.J. Piermarini, Pressure-temperature phase diagram of zirconia, J. Am. Ceram. Soc. (1985) 497–499.
- [42] X.J. Jin, Martensitic transformation in zirconia containing ceramics and its applications, Curr. Opin. Solid State Mater. Sci. 9 (2005) 313–318, http://dx. doi.org/10.1016/j.cossms.2006.02.012.
- [43] M. Lerch, Nitridation of Zirconia, J. Am. Ceram. Soc. 79 (10) (2005) 2641–2644, http://dx.doi.org/10.1111/j.1151-2916.1996.tb09028.x.
- [44] Y. Cheng, D.P. Thompson, Nitrogen-containing tetragonal zirconia, J. Am. Ceram. Soc. 74 (5) (1991) 1135–1138, http://dx.doi.org/10.1111/j.1151-2916.1991. tb04355.x.
- [45] Y.-B. Cheng, D.P. Thompson, Role of anion vacancies in nitrogen-stabilized zirconia, J. Am. Ceram. Soc. 76 (3) (1993) 683–688, http://dx.doi.org/10.1111/ j.1151-2916.1993.tb03660.x.
- [46] F. Humphreys, M. Hatherly, Recrystallization and Related Annealing Phenomena, Elsevier, Oxford, 2004.